Modeling vertical stratification of CO_2 injected into a deep layered aquifer

Mohamed Hayek *, Emmanuel Mouche, Claude Mügler

Laboratoire des Sciences du Climat et de l'Environnement, UMR, CEA-CNRS-UVSQ, Centre d'Etudes de Saclay, Orme des Merisiers, F-91191 Gif-sur-Yvette Cedex, France

ARTICLE INFO

ABSTRACT

The vertical stratification of carbon dioxide (CO_2) injected into a deep layered aquifer made up of high-permeability and low-permeability layers, such as Utsira aquifer at Sleipner site in Norway, is investigated with a Buckley–Leverett equation including gravity effects. In a first step, we study both by theory and simulation the application of this equation to the vertical migration of a light phase (CO_2), in a denser phase (water), in 1D vertical columns filled with different types of porous media: homogeneous, piecewise homogeneous, layered periodic and finally heterogeneous. For each case, we solve the associated Riemann problems and propose semi-analytical solutions describing the spatial and temporal evolution of the light phase saturation. These solutions agree well with simulation results. We show that the flux continuity condition at interfaces between high-permeability and low-permeability layers leads to CO_2 saturation discontinuities at these interfaces and, in particular, to a saturation increase beneath low-permeability layers. In a second step, we analyze the vertical migration of a CO_2 plume injected into a 2D layered aquifer. We show that the CO_2 vertical stratification under each low-permeability layer is induced, as in 1D columns, by the flux continuity condition at interfaces. As the injection takes place at the bottom of the aquifer the velocity and the flux function decrease with elevation and this phenomenon is proposed to explain the stratification under each mudstone layer as observed at Sleipner site.

© 2008 Elsevier Ltd. All rights reserved.

1. Introduction

Underground injection and long-term storage of carbon dioxide (CO_2) is now recognized as one possible method to reduce CO_2 emissions to the atmosphere. Candidate sites for injection include geologic formations such as petroleum reservoirs [15,18,19] and deep saline aquifers [4,14,17]. The former are preferred due to their proven seal, but the latter are much more common worldwide. Unfortunately, aquifers are much less characterized than petroleum reservoirs and there is normally no proof that the caprock is perfectly impervious. Characterization of the aquifer is an important part of the total evaluation of the aquifer as a reliable long-term CO_2 sequestration site.

An ongoing project is the Sleipner project in Norway which has demonstrated the feasibility of industrial CO_2 injection into the Utsira saline aquifer of Sleipner Vest field [31] ($\sim 10^6$ tons/year). This site is located in the Norwegian sector of the North Sea, where about 8 million tons of CO_2 have been injected since 1996 into the Utsira Sand, an approximately 200-m thick saline aquifer located at a depth of 1012 m below sea level. CO_2 is injected at the bottom of the aquifer and migrates under the combined action of injection and gravity (Fig. 1). At the aquifer conditions, CO_2 is less dense than

the aquifer brine and therefore rises buoyantly. By 1999, the CO_2 appeared to have reached the top of the reservoir. Well and seismic data obtained prior to the injection showed that the aquifer sandstone is divided by nearly horizontal discontinuous thin mudstone layers [21]. Seismic profiles measured in 1999, 2001 and 2002 showed large increase in reflectivity indicating individual CO_2 accumulations under mudstone layers (Fig. 2).

Mathematical models and numerical simulation tools play an important role to evaluate the feasibility of CO_2 storage in subsurface reservoirs, to design and analyze field tests, and to design and operate geologic CO_2 disposal systems. Numerical simulators can solve complex partial differential equations that describe the physics realistically, but the accuracy of results depend both on numerical scheme and spatial and time discretizations. In recent years, a lot of research work dealt with numerical simulation of CO_2 injection processes into geological formations [6,25,27,28], see for instance the international project Geoseq, initiated a few years ago by the Lawrence Berkeley National Laboratory in the USA [29].

On the other hand, semi-analytical models have been developed to provide solutions, either for code validation or for a better understanding of flow and migration processes at the different space and time scales of interest. Recently, different authors developed sharp-interface models to study the CO_2 plume dynamics during and after injection. The sharp-interface relies on two main assumptions (e.g. [12]): (i) the fluids are completely segregated and therefore separated by a sharp-interface, (ii) pressure is hydrostatic in both fluids

---

* Corresponding author.
  E-mail addresses: mohamed.hayek@lsce.ipsl.fr, mohamed.hayek@gmail.com (M. Hayek).
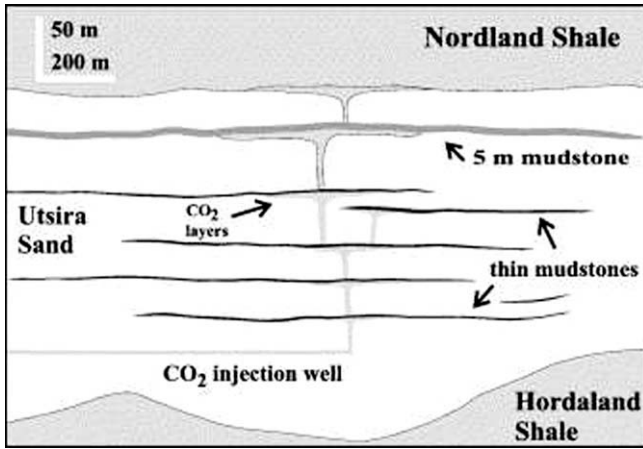
Fig. 1. Schematic illustration of CO_2 injection at Sleipner and rising CO_2 plumes being partially trapped under thin mudstones before reaching Nordland Shale caprock. Note the vertical exaggeration (after Bickle et al. [5]).

and flow is parallel to the aquifer boundary. Following this approximation, Nordbotten et al. [24] developed an analytical solution for CO_2 injection into aquifers, and proved through an intercomparison exercise with the simulator ECLIPSE developed by Schlumberger (Schlumberger Information Systems), that this solution captures well the migration process for different storage conditions. In a first paper, Hesse et al. [12] studied the plume dynamics during and after injection by means of similarity solutions. In a second paper [13], they studied the long-term migration of the CO_2 plume in a sloping aquifer and assessed the impact of residual trapping. These models can be also fast and efficient tools to model experimental results and infer storage properties as showed by Bickle et al. [5] in their modeling work on Sleipner injection experiment. They used an analytical solution developed by Lyle et al. [22] for an axisymmetric geometry to discuss the dynamics of CO_2 accumulation observed on the site, i.e. growth of CO_2 layers radii and thicknesses, under each mudstone layer as imaged by seismic reflection profiles.

All these sharp-interface models address the issue of CO_2 horizontal spreading under an impervious layer. As the fluid relative-permeabilities are neglected, they cannot be used to study the CO_2 vertical migration through the different Utsira layers, and the progressive stratification observed at the site.

In this paper, we propose a theoretical investigation, supported by numerical simulation, of the CO_2 vertical migration in layered porous media of Sleipner type. The equation governing CO_2 saturation is a Buckley–Leverett equation with gravity [3,9,11]. Very few theoretical works have been done on this type of equation in heterogeneous porous media and most of the existing works investigated, partially, the Riemann problems at the interface between

two porous media and addressed the related numerical issues. We can cite for instance Kaasschieter [16] or Adimurthi et al. [1] who studied the Riemann problem raised by the flux discontinuity at the interface of two porous media and proposed numerical strategies, based on Godunov method, to solve the problem.

We study in a first step the migration of a CO_2 gas zone in a vertical column filled with a homogeneous porous medium. Then, the saturation evolution at the interface of two different porous media is analyzed and the associated Riemann problems are solved. The flux continuity imposed at this interface implies a saturation discontinuity. Then, depending on the flux value, the CO_2 accumulates or/and passes through the interface. We derive a semi-analytical solution for the case of one-dimensional layered porous medium which describes the spatial and temporal evolution of the saturation through the column. The study is extended to the two-dimensional case, 2D vertical cut of a periodic layered aquifer, and we propose an explanation of the observed CO_2 stratification in the Utsira aquifer.

2. Incompressible and immiscible two-phase flow model

The flow of two incompressible fluids, water and CO_2, in a porous medium is described by the saturation equation and the generalized Darcy law of the liquid (water) and gas (CO_2) fluid phases. The saturation equation of phase α is given by [3]:

$$\phi \frac{\partial S_\alpha}{\partial t} + \nabla \cdot \mathbf{v}_\alpha = q_\alpha, \quad \alpha = w, g, \tag{1}$$

where ϕ is the porosity of the medium, S_α, $\mathbf{v}_\alpha$ and q_α the saturation, the generalized Darcy velocity and the sink/source term of phase α, respectively. The subscripts w and g denote the gas and water phases, respectively, $\nabla \cdot = \left(\frac{\partial}{\partial x}, \frac{\partial}{\partial z}\right)^\top$ is the divergence operator, x and z denote the coordinates in the horizontal and vertical directions. In this paper, we assume that both fluids are incompressible. Indeed, the vertical extent where the solution is analyzed (between two low-permeability layers) is not too large relative to the absolute depth, so the variation of the hydrostatic pressure is not large.

The velocity $\mathbf{v}_\alpha$ is described by the generalized Darcy law as follows:

$$\mathbf{v}_\alpha = -\frac{kk_{r\alpha}}{\mu_\alpha} \nabla(p_\alpha + \rho_\alpha g z), \quad \alpha = w, g, \tag{2}$$

where k is the absolute permeability of the porous medium, g the gravity acceleration, p_α, ρ_α, $k_{r\alpha}$ and μ_α the pressure, density, relative-permeability and viscosity of phase α, respectively. The phase saturations are constrained by:

$$S_w + S_g = 1 \tag{3}$$

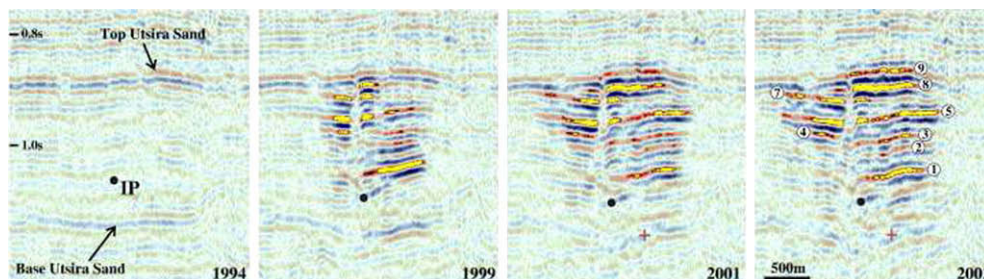and the two-phase pressures are related by the capillary pressure (p_c) function:

Fig. 2. Seismic reflection profiles in 1994, 1999, 2001 and 2002. The 1994 pre-injection profile shows the base and top of the Utsira Sand but little detail within the reservoir. The subsequent post-injection profiles show bright reflections where CO_2 is ponding under thin mudstones. Note the pushdown of the basal Utsira Sand reflection resulting from low velocity of CO_2 in the reservoir and development of a low amplitude vertical "chimney" just to left (south) of the injection point (IP) presumed to be the main vertical conduit of CO_2 in the plume. Layers are numbered in 2002 profile (after Bickle et al. [5]).

$$p_c(S_g) = p_g - p_w. \tag{4}$$

To eliminate the unknown pressure gradient, following the fractional flow theory, we use the total flow velocity [11]:

$$\mathbf{v} = \mathbf{v}_g + \mathbf{v}_w. \tag{5}$$

The gas phase velocity $\mathbf{v}_g$ can be expressed as a function of the total velocity and the capillary pressure gradient by using Eqs. (2), (4) and (5):

$$\mathbf{v}_g = \frac{\lambda_g}{\lambda_g + \lambda_w}\mathbf{v} + k\frac{\lambda_g\lambda_w}{\lambda_g + \lambda_w}(\rho_w - \rho_g)g\nabla z - k\frac{\lambda_g\lambda_w}{\lambda_g + \lambda_w}\nabla p_c. \tag{6}$$

In Eq. (6), $\lambda_\alpha = \frac{k_{r\alpha}}{\mu_\alpha}$ is the mobility of phase α.

Since the solubility of the supercritical CO_2 in water is low, we can neglect it during the injection phase which is studied in this paper. The three terms in Eq. (6) correspond to the three driving forces of the CO_2 plume vertical migration: injection, gravitation and capillarity. In this paper, we consider the two first forces (injection and gravitation) and capillarity is neglected. In the framework of this assumption, the proposed model (without capillarity) allows to explain the CO_2 vertical stratification in a deep layered aquifer. Then, with this assumption and after substitution of Eq. (6) into Eq. (1) for $\alpha = g$, we obtain the saturation equation of the gas phase as a balance equation:

$$\phi\frac{\partial S_g}{\partial t} + \nabla \cdot \mathbf{F}(S_g) = q_g, \tag{7}$$

where

$$\mathbf{F}(S_g) = f(S_g)[\mathbf{v} + k(\rho_w - \rho_g)g\lambda_w(S_g)\nabla z] \tag{8}$$

is the global flux function and $f(S_g) = \frac{\lambda_g}{\lambda_g + \lambda_w}$ is the fractional flow (flux) function of the gas phase.

Adding the two-phase saturation equations given in Eq. (1) and using Eqs. (3) and (5), we obtain for $q_w = 0$:

$$\nabla \cdot \mathbf{v} = q_g. \tag{9}$$

According to Eqs. (2) and (5), the total velocity $\mathbf{v}$ can be expressed in terms of the gas pressure gradient as follows:

$$\mathbf{v} = -k(\lambda_g + \lambda_w)\nabla p_g - k(\lambda_g\rho_g + \lambda_w\rho_w)g\nabla z. \tag{10}$$

The system of Eqs. (7)–(10) is solved with appropriate initial and boundary conditions which describe the initial saturation, boundary pressure and external flow rate. Let $\Gamma = \Gamma^D \cup \Gamma^N$ be the boundary of the computational domain Ω, where Γ^D and Γ^N are non-overlapping boundaries corresponding to Dirichlet and Neumann boundary conditions. The saturation equation (7) is subject to the following initial and boundary conditions:

$$\begin{aligned} S_g &= S^0, \text{ in } \Omega, \\ S_g &= S^N, \text{ on } \Gamma^N, \end{aligned} \tag{11}$$

and the balance equation (9) is subject to:

$$\begin{aligned} p_g &= p^D, \text{ on } \Gamma^D, \\ \mathbf{v} \cdot \mathbf{n} &= q^N, \text{ on } \Gamma^N, \end{aligned} \tag{12}$$

where S^0 is the initial saturation, S^N the boundary saturation of the injected fluid (CO_2) at Γ^N, p^D and q^N the imposed pressure and injected rate at Γ^D and Γ^N, respectively, and $\mathbf{n}$ the outward unit normal vector.

Index g is now omitted in the system of Eqs. (7)–(12) and $S = S_g$ represents the gas (CO_2) saturation.

The resolution of system (7)–(12) requires the knowledge of relative-permeability laws. We assume that relative-permeabilities depend on the gas saturation only:

$$k_{r\alpha} = k_{r\alpha}(S), \quad \alpha = g, w. \tag{13}$$

Many relative-permeability laws exist in the literature. They are usually written as functions of the effective gas phase saturation:

$$S_{eg} = \frac{S - S_{rg}}{1 - S_{rg} - S_{rw}}, \tag{14}$$

where $S_{r\alpha}$ ($\alpha = g, w$) is the relative (or irreducible) saturation of phase α.

The most used relative-permeability laws for CO_2 migration in geological media are the Brooks–Corey [7] and van Genuchten [32] laws. In this work, we use the Brooks–Corey relative-permeability laws which are defined by:

$$\begin{aligned} k_{rw}(S) &= (1 - S_{eg})^{\frac{2+3\lambda}{\lambda}}, \\ k_{rg}(S) &= S_{eg}^2\left[1 - (1 - S_{eg})^{\frac{2+\lambda}{\lambda}}\right], \end{aligned} \tag{15}$$

where λ is the pore size distribution index. In this paper, we take $\lambda = 2$ which corresponds to Corey model.

The model is solved with the numerical code (Cast3M) developed by the french Atomic Energy Commission (CEA) (see the website www-cast3m.cea.fr for more information about Cast3M). A Mixed-Hybrid Finite Element (MHFE) formulation is used to solve the general flow Eqs. (9) and (10) and the advection term in Eq. (7) is discretized with a classical upwind scheme. The time discretization is implicit and the nonlinear terms are solved with an iterative Picard algorithm. The coupling between the flow and the saturation transport equations is sequential-iterative.

3. Injection and migration in a vertical column

In order to analyze the vertical migration of a CO_2 plume in a 2D heterogeneous aquifer, we consider in a first step the migration of a plume injected into a vertical column filled with different types of porous media and initially saturated with water. For simplification, we assume that the porosity ϕ is constant. Then, the governing equation is obtained by writing Eq. (7) along the vertical direction:

$$\frac{\partial S}{\partial t} + \frac{\partial}{\partial z}F(S) = \frac{q_g}{\phi}, \tag{16}$$

where

$$F(S) = \frac{1}{\phi}f(S)\left[v + \frac{k(\rho_w - \rho_g)g}{\mu_w}k_{rw}(S)\right] \tag{17}$$

is the global flux function. In this case where the geometry is 1D and vertical, the total velocity v is constant. This saturation equation with the global flux function is the Buckley–Leverett equation with gravity [3,9,11].

First, we consider the homogeneous case where k is constant and we apply the method introduced by Proskurowski [26] to construct the solution of the Riemann problem associated to the Buckley–Leverett equation (16). Then, we study the solution behavior at a permeability discontinuity. Finally, we consider the injection in a column filled with a heterogeneous layered porous media. Semi-analytical solutions are derived and compared to numerical ones. In all cases, we use the Brooks–Corey relative-permeability laws and assume that $S_{rg} = S_{rw} = 0$. The physical parameters of the test cases are given in Table 1.

3.1. Homogeneous porous medium

In the case of an injection in a homogeneous porous medium, the migration regime depends mainly on two parameters, the injection rate v and the mean ascent velocity:

$$G = \frac{k(\rho_w - \rho_g)g}{\mu_w}\overline{k_{rw}}, \tag{18}$$

Table 1
Fluid properties and parameters of column simulations.

Porous media properties:

ϕ	All cases: 0.35
$k\ (m^2)$	Homogeneous case: 3×10^{-12}
	Case (1a): $k_1 = 10^{-13}$, $k_2 = 5 \times 10^{-14}$
	Case (1b): $k_1 = 5 \times 10^{-14}$, $k_2 = 10^{-13}$
	Case (2a): $k_1 = 2 \times 10^{-13}$, $k_2 = 10^{-13}$
	Case (2b): $k_1 = 10^{-13}$, $k_2 = 2 \times 10^{-13}$
	Periodic column: $k_1 = 10^{-13}$, $k_2 = 5 \times 10^{-14}$
	Non-periodic column: $k_1 = 2 \times 10^{-13}$, $k_2 = 10^{-13}$,
	$k_3 = 5 \times 10^{-14}$

Fluid properties:

$\rho_w\ (kg\ m^{-3})$	997.42
$\rho_g\ (kg\ m^{-3})$	716.7
$\mu_w\ (kg\ m^{-1}\ s^{-1})$	5.98×10^{-4}
$\mu_g\ (kg\ m^{-1}\ s^{-1})$	5.98×10^{-4}
S_{rw}	0.0
S_{rg}	0.0
k_{rw}	Brooks–Corey
k_{rg}	Brooks–Corey

Initial conditions:

S^0	0.0

Well boundary condition:

S^N	1.0
$v\ (m\ s^{-1})$	Homogeneous case: 0.0
	Cases (1a), (1b), periodic and non-periodic column:
	2.21×10^{-8}
	Cases (2a) and (2b): 4.42×10^{-7}

Spatial discretization:

Grid resolution Δz (m)	1.2×10^{-3}

where

$$\overline{k_{rw}} = \frac{1}{1 - S_{rg} - S_{rw}} \int_{S_{rg}}^{1-S_{rw}} k_{rw}(S)\, dS \qquad (19)$$

is the averaged relative-permeability of the water phase. Let us introduce the dimensionless parameter $\theta = \frac{v}{G}$, similar to the gravity number introduced by Riaz and Tchelepi [30]. If $\theta \gg 1$, the plume ascent is essentially injection driven and does not depend on the absolute permeability. On the contrary, if $\theta \ll 1$, the ascent is buoyancy driven and depends on the absolute permeability.

With the relative-permeability laws presented in Section 2, the function f is a monotonic increasing "S-shaped" function. The shape of the global flux F depends on the value of θ. Indeed, if $\theta \gg 1$, function F is also a "S-shaped" function, and if $\theta \ll 1$, it is
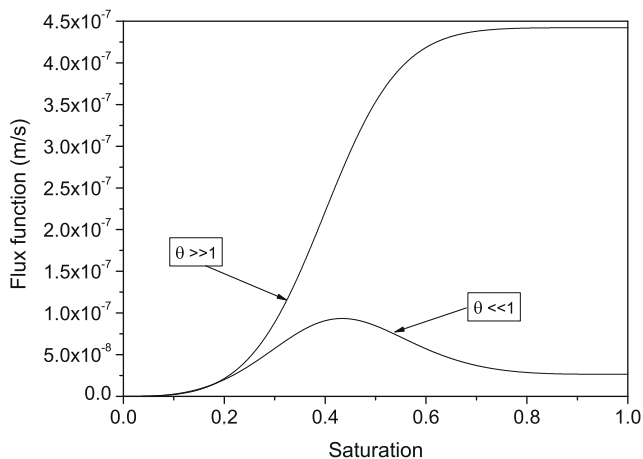

Fig. 3. General shapes of the flux function F for the two cases: injection driven ($\theta \gg 1$) and buoyancy driven ($\theta \ll 1$).

a "bell-shaped" function. The general shapes of function F are displayed in Fig. 3 for the two cases $\theta \gg 1$ and $\theta \ll 1$.

In the injection driven case ($\theta \gg 1$) we have $F(S) \simeq \frac{1}{\phi} f(S)\,v$, and Eq. (16) corresponds to the well known Buckley–Leverett equation [8]. The solution of this equation can be obtained with the Welge tangent method [11].

In the buoyancy driven case ($\theta \ll 1$), Eq. (16) corresponds to the Buckley–Leverett problem with gravity [2,23,26,33] and the global flux $F(S)$ displays two inflection points as shown in Fig. 3. The solution of the corresponding Riemann problem can be constructed from the convex or/and concave hull(s) of the flux function [2,9,10,26]. We follow here the method proposed by Proskurowski [26]. This method is applied to the problem of a CO_2 plume which migrates in a homogeneous column under the action of buoyancy only ($\theta = 0$).

3.1.1. Solution of the Riemann problem

A Riemann problem is defined by a saturation equation (16) with an initial saturation discontinuity at one point. If this initial discontinuity is located at $z = \xi$ with two constant states, an upstream state $S_u = \lim_{z \to \xi^-} S(z, t = 0)$ and a downstream one $S_d = \lim_{z \to \xi^+} S(z, t = 0)$, the solution will travel as a rarefaction wave(s) and/or as a shock(s). Let $S^- = \lim_{z \to \xi^-} S(z, t)$ and $S^+ = \lim_{z \to \xi^+} S(z, t)$ be the limiting values from the left and the right, respectively, at the discontinuity. To obtain a unique weak solution (i.e. the physical solution) of the Riemann problem, the following conditions must hold along any curve of discontinuity of $S(z, t)$:

- (i): The Rankine–Hugoniot jump condition (see, for example, [2]): the curve of discontinuity is a straight line with slope $\sigma_{-,+} = \frac{F(S^+) - F(S^-)}{S^+ - S^-}$.
- (ii): The entropy condition (see, for example, [11]): $\frac{F(S) - F(S^-)}{S - S^-} \geqslant \sigma_{-,+} \geqslant \frac{F(S) - F(S^+)}{S - S^+}$, for any S between S^- and S^+.

Graphically, the solution of the Riemann problem with an initial saturation discontinuity defined by S_u and S_d can be constructed as follows:

- (I): If $S_u < S_d$ then we construct the convex hull $\check{F}$ of F over $[S_u, S_d]$. The part(s) of $\check{F}$ constituted by straight lines represent(s) the shock(s), and the part(s) of $\check{F}$ which coincide(s) with the graph of F represent(s) the rarefaction wave(s).
- (II): If $S_u > S_d$ then we construct the concave hull $\widehat{F}$ of F over $[S_d, S_u]$. The part(s) of $\widehat{F}$ constituted by straight lines represent(s) the shock(s), and the part(s) of $\widehat{F}$ which coincide(s) with the graph of F represent(s) the rarefaction wave(s).

Let us note that if two saturation values are connected by a shock, they verify condition (ii) and this shock travels with a velocity $\sigma_{-,+}$ given by (i).

3.1.2. Dynamics of a CO_2 plume under the action of gravity alone

Few authors have investigated the unidimensional vertical dynamics of a light phase in a denser one. One may cite for instance the recent work of Cunha et al. [10] who performed a laboratory experiment to analyze the motion of gas (atmospheric air) and liquid in a porous medium under the condition of vertical equilibrium, i.e. the total velocity equal to zero.

In our application the gas is CO_2 and the plume is initially located between $z_1 = 2$ m and $z_2 = 4$ m in a 7-m long column with an initial saturation $S^0 = 0.7$. With the vertical equilibrium condition, i.e. $v = 0$, the plume rises under the action of buoyancy only. The flux function has the bell shape shown in Fig. 4a.

This example exhibits two Riemann problems, the first one is located at $z = z_1$ with $S_d = S^0$ and $S_u = 0$ and the second one at $z = z_2$ with $S_d = 0$ and $S_u = S^0$. For the first problem, we consider

the convex hull of the flux function and apply item (I); then the solution is made of a rarefaction wave (r_1) and a shock (s_1) which both travel upward. For the second problem, the concave hull is considered and item (II) is applied; then two shocks (s_2) and (s_3) traveling in opposite directions are created, separated by a rarefaction wave (r_2). Fig. 4a summarizes graphically this resolution method.

Fig. 4b shows a comparison between numerical and semi-analytical solutions at a short time. The semi-analytical solution is obtained as follows: a saturation S which belongs to a rarefaction wave, (r_1) or (r_2), travels at a velocity v_S equal to $F'(S)$ and its trajectory is given by the method of characteristics [3]: $z_S = z_S(0) + F'(S)t$. Each shock (s_1, s_2, s_3) travels with a velocity equal to the slope of the straight line which connects the saturation values at each side of the considered discontinuity (Fig. 4b). As we remark in this figure, the velocity of (s_3) is greater than that of (s_1), indicating that the plume spreads. As shocks (s_1) and (s_2) propagate in opposite directions, the area of the plume saturated with $S = S^0$ shrinks as time increases and disappears when (s_1) and (s_2) meet together. We can remark the good agreement between semi-analytical solution and simulation.

3.2. Piecewise homogeneous porous medium

The influence of permeability heterogeneity on the solution of the Buckley–Leverett equation with gravity is rarely studied in the literature. We can cite the works of Kaasschieter [16], Langtan-

Fig. 4. CO_2 plume migration in a vertical column filled with a homogeneous porous medium: (a) construction of the convex and concave hulls for a plume of initial saturation S^0; (b) analytical and numerical solutions at a short time.

gen et al. [20] or Adimurthi et al. [1] who solve theoretically and/or numerically the Riemann problems associated to the Buckley–Leverett equation with a permeability discontinuity and in presence of gravity. In their studies, the discontinuity location is the same for both the initial saturation and the permeability. This assumption is quite restrictive and does not allow to analyze the problem of a plume migration through a permeability distribution.

In this section, we consider the injection of CO_2 at the bottom of a vertical 6-m long column filled with a composite porous medium. Region 1 $(z < z_0)$ is filled with medium 1 and region 2 $(z > z_0)$ with medium 2, where $z_0 = 3$ m is the interface location. We note k_i and F_i the absolute permeability and the flux function of porous medium i, respectively. Both media have the same Brooks–Corey relative-permeability. The CO_2 migration regime depends on two dimensionless parameters: $\bar{\theta} = \max(\theta_1, \theta_2)$, where $\theta_i = \frac{v}{G_i}$ with v being the injection rate and G_i the mean ascent velocity given by Eq. (18), and the ratio $r = \frac{k_1}{k_2}$. According to Section 3.1, the migration regime is buoyancy driven when $\bar{\theta} \ll 1$ and it is injection driven when $\bar{\theta} \gg 1$. Therefore, we distinguish four cases of interest:

- Case (1a): $\bar{\theta} \ll 1$ and $r > 1$.
- Case (1b): $\bar{\theta} \ll 1$ and $r < 1$.
- Case (2a): $\bar{\theta} \gg 1$ and $r > 1$.
- Case (2b): $\bar{\theta} \gg 1$ and $r < 1$.

In all these cases, we assume $S_{rg} = S_{rw} = 0$ and $S(0, t) = 1$ (fixed saturation at the bottom of the column $z = 0$). For cases (1a) and (1b), we note $S_{max,i}$ the saturation for which F_i is maximum $(i = 1, 2)$. We note S_{wi} the saturation such that the straight line joining $(S = 0, F_i(0))$ to $(S_{wi}, F_i(S_{wi}))$ in the $(S, F(S))$ plane is tangent to $F_i(S_{wi})$ $(i = 1, 2)$. When $\bar{\theta} \ll 1$ this straight line is the Welge tangent.

3.2.1. Case (1a): Buoyancy driven and $k_1 > k_2$

Initially, the saturation discontinuity is located at the injection point $(z = 0)$, with $S_u = 1$ and $S_d = 0$. Then, according to item (II) of Section 3.1, we consider the concave hull $\widehat{F}_1$ of F_1 over $[0, 1]$ (Fig. 5a). For saturations $S > S_{max,1}$, we have $\widehat{F}'_1(S) < 0$, therefore these saturations travel downward. Since injection takes place at the bottom in the ascending direction, only saturations defined by $S \in [0, S_{max,1}]$ must be considered. Consequently, the solution is made of a rarefaction wave (r_1) from $S = S_{max,1}$ to $S = S_{w1}$ and a shock (s_{11}) from $S = S_{w1}$ to $S = 0$.

For $z < z_0$ and $t > 0$, each saturation of the rarefaction wave (r_1), $S(z, t) \in [S_{w1}, S_{max,1}]$, is described by the trajectory $z_S(t) = F'_1(S(z, t))t$ and the shock location is given by $z(t) = \frac{F_1(S_{w1})}{S_{w1}}t$. CO_2 reaches the interface between the two regions $(z = z_0)$ at $t^* = \frac{z_0 S_{w1}}{F_1(S_{w1})}$.

For $t > t^*$, the flux must be continuous at the interface. This condition leads to a saturation discontinuity at this interface defined by $S^-(z_0, t) = \lim_{z \to z_0^-} S(z, t)$ and $S^+(z_0, t) = \lim_{z \to z_0^+} S(z, t)$, and such that $F_1(S^-(z_0, t)) = F_2(S^+(z_0, t))$. Langtangen et al. [20] and Kaasschieter [16] propose entropy conditions to determine the evolution of the discontinuity which is solution of the Riemann problem at the interface. These entropy conditions are derived from a regularization procedure, where a small diffusion term is added to the saturation equation. In order to determine $S^-(z_0, t)$ and $S^+(z_0, t)$ at each time $t > t^*$, we use results obtained by Kaasschieter [16].

The construction of the solution is illustrated in Fig. 5a. Let us call $S_1(z, t)$ the saturation computed in the homogeneous porous column case $(k_1 = k_2)$ at time t. For $t < t^*$, $S(z, t) = S_1(z, t)$ and for $t \geqslant t^*$, $S_1(z_0, t)$ is the saturation arriving at $z = z_0$ at time t. According to the time evolution previously described, we have $S_{w1} \leqslant S_1(z_0, t) \leqslant S_{max,1}$. Then, the flux at the interface is greater than the maximal flux in medium 2 (see Fig. 5a). Continuity of flux at the interface can only be satisfied if the flux at this interface is reduced to a value equal to the maximal flux of medium 2. Then,
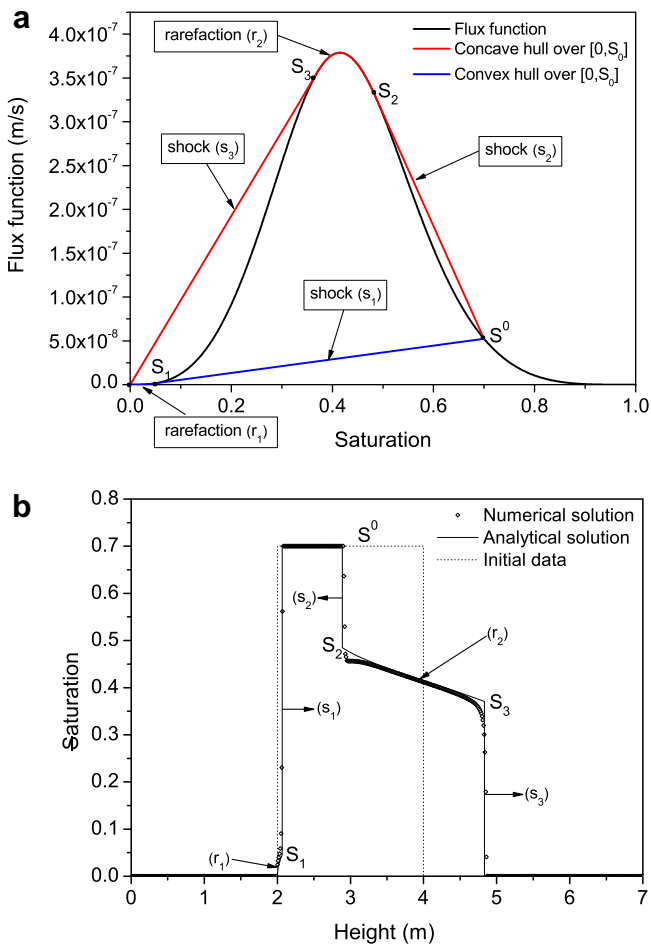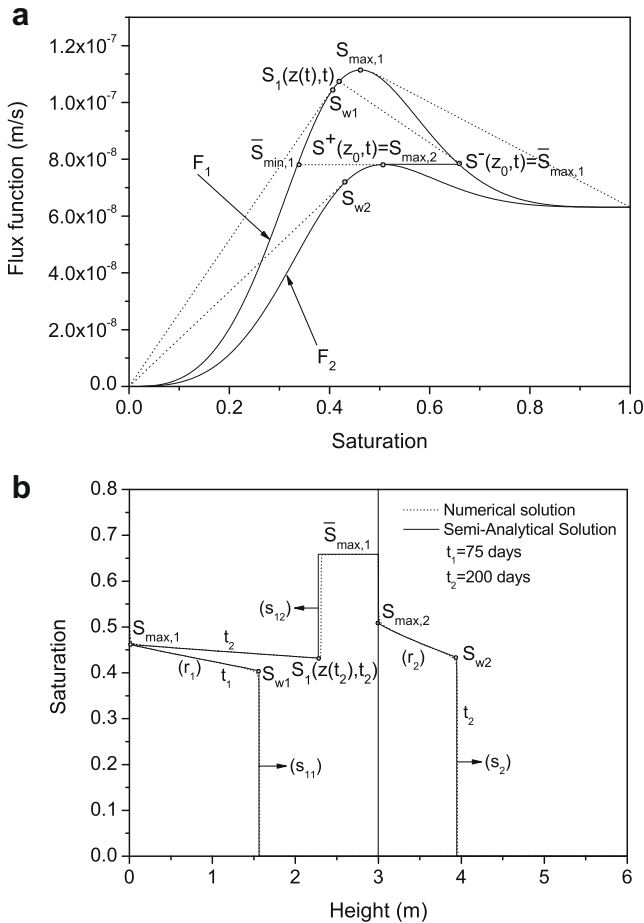
Fig. 5. CO_2 migration in a vertical column filled with a piecewise homogeneous porous medium. Case (1a) buoyancy driven ($\bar{\theta} \ll 1$) and medium one (left) is more permeable than medium two (right) ($r > 1$). (a) Flux curves, concave and convex hulls; (b) numerical and semi-analytical solutions.

$S^+(z_0, t) = S_{max,2}$, value for which F_2 is maximum, and $S^-(z_0, t) = \bar{S}_{max,1} > S^+(z_0, t)$ where $\bar{S}_{max,1}$ is defined by the flux equality $F_1(\bar{S}_{max,1}) = F_2(S_{max,2})$ (see Fig. 5a). The other solution $\bar{S}_{min,1}$ is disregarded since it does not satisfy the entropy condition (see Kaasschieter [16] for more details).

Therefore, at $t \geqslant t^*$, we have to solve a Riemann problem in region 1 and another one in region 2. In medium 1, we consider the convex hull over $[S_1(z(t), t), \bar{S}_{max,1}]$ and, according to item (I), $S_1(z(t), t)$ is connected to $\bar{S}_{max,1}$ by a shock (s_{12}) which travels downward with a velocity $v(t) \equiv v(z(t)) = \frac{F_1(\bar{S}_{max,1}) - F_1(S_1(z(t),t))}{\bar{S}_{max,1} - S_1(z(t),t)} < 0$, where $z(t)$ is the shock front location given by the implicit relationship $z(t) = z_0 + \int_{t^*}^t v(z(t'))dt'$. In medium 2, we have at the interface at $t = t^*$, $S_u = S_{max,2}$ and $S_d = 0$, then, according to item (II), we consider the concave hull over $[0, S_{max,2}]$. The solution is made of a rarefaction wave (r_2) from $S = S_{max,2}$ to $S = S_{w2}$, and a shock (s_2) from $S = S_{w2}$ to $S = 0$. This shock is located at $z(t) = z_0 + \frac{F_2(S_{w2})}{S_{w2}}(t - t^*)$. Fig. 5b shows numerical and semi-analytical solutions at two different times $t_1 < t^*$ and $t_2 > t^*$.

We remark that in this case, when the CO_2 plume reaches the interface between medium 1 and medium 2 at $t = t^*$, the CO_2 starts to accumulate in medium 1 beneath the interface. At this time, the saturation at the interface in medium 1 becomes constant and equal to $\bar{S}_{max,1}$. At the same time, the CO_2 plume penetrates into medium 2 and the saturation jumps from $\bar{S}_{max,1}$ to $S_{max,2}$. Then, the zone in medium 1 where $S = \bar{S}_{max,1}$ increases with time until saturation becomes equal to $\bar{S}_{max,1}$ in all medium 1.

3.2.2. Case (1b): Buoyancy driven and $k_1 < k_2$

For $t < t^*$, the solution is the same as in case (1a). For $t \geqslant t^*$, flux continuity implies again a saturation discontinuity at the interface. With the definitions and notations of case (1a) the solution is given by the following equalities: for $z < z_0$, $S(z, t) = S_1(z, t)$, $S^-(z_0, t) = S_1(z_0, t)$ and $S^+(z_0, t)$ is given by $F_1(S^-(z_0, t)) = F_2(S^+(z_0, t))$. Then, we have $S^-(z_0, t) > S^+(z_0, t)$ (Fig. 6a).

For $t \geqslant t^*$, we have a Riemann problem in medium 2 at the interface with $S_u = S^+(z_0, t)$ and $S_d = 0$. According to item (II), we consider the concave hull over $[0, S^+(z_0, t)]$. Since $S^+(z_0, t) < S_{w2}$, this concave hull is a straight line (Fig. 6a) and a shock (s_2) is created between $S = S^+(z_0, t)$ and $S = 0$. This shock travels upward with a velocity $v(t) = \frac{F_2(S^+(z_0,t))}{S^+(z_0,t)} > 0$. This means that at any time $t > t^*$ the saturation in medium 2 looks like a convected step function: the saturation is independent of z and equal to $S^+(z_0, t)$, the saturation front travels at a velocity $v(t)$ and its position is equal to $z(t) = z_0 + \int_{t^*}^t v(t')dt'$. Fig. 6 shows numerical and semi-analytical solutions for two different times $t_1 < t^*$ and $t_2 > t^*$.

3.2.3. Case (2a): Injection driven and $k_1 > k_2$

For the saturation discontinuity at the origin, we consider the concave hull $\hat{F}_1$ of F_1 over $[0, 1]$. Since $F_1'(S) \geqslant 0$ for $S \in [0, 1]$, the solution is made of a rarefaction wave (r_1) from $S = 1$ to $S = S_{w1}$ and a shock (s_{11}) from $S = S_{w1}$ to $S = 0$ (Fig. 7a).

At $t = t^*$, a saturation discontinuity takes place at the interface between $S^-(z_0, t^*) = S_1(z_0, t^*) = S_{w1}$ and $S^+(z_0, t^*) = S^*$, where S^* satisfies $F_1(S_{w1}) = F_2(S^*)$ (Fig. 7a). In region 2, always at $t = t^*$, we con-
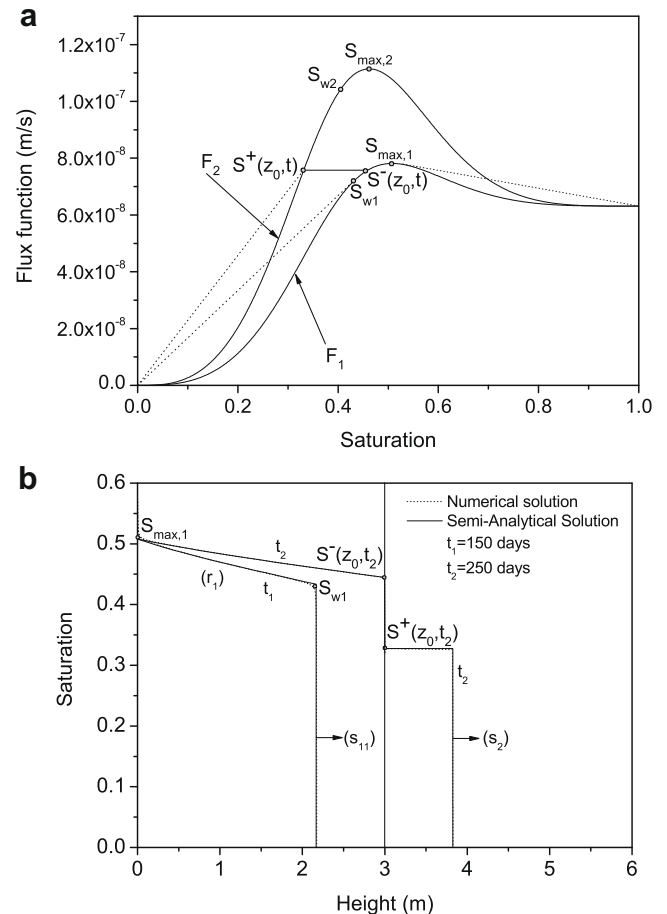

Fig. 6. CO_2 migration in a vertical column filled with a piecewise homogeneous porous medium. Case (1b) buoyancy driven ($\bar{\theta} \ll 1$) and medium two (right) is more permeable than medium one (left) ($r < 1$). (a) Flux curves, concave and convex hulls; (b) numerical and semi-analytical solutions.

sider the concave hull between $S_u = S^*$ and $S_d = 0$, then a rarefaction wave (r_{22}) is created between $S = S^*$ and $S = S_{w2}$ and a shock (s_2) from $S = S_{w2}$ to $S = 0$. A saturation which belongs to (r_{22}) travels at a velocity equal to $F'_2(S)$ and its trajectory is given by the method of characteristics: $z_S = z_0 + F'_2(S)(t - t^*)$.

For $t \geqslant t^*$, we have $F_1(S_1(z_0,t)) = F_2(S^+(z_0,t))$ where $S^+(z_0,t) > S^*$. Then, a rarefaction wave (r_{21}) is created between $S^+(z_0,t)$ and S^*, see Fig. 7a. A saturation S_2 which belongs to (r_{21}) is described by the trajectory: $z_{S_2} = z_0 + F'_2(S_2)(t - t_{S_2})$ where $t_{S_2} = \frac{z_0}{F'_1(S_1)}$ and the saturation S_1 in region 1 is such that $F_1(S_1) = F_2(S_2)$. A comparison between numerical and semi-analytical solutions presented in Fig. 7b shows a good agreement.

3.2.4. Case (2b): Injection driven and $k_1 < k_2$

For $t < t^*$, the solution is the same as in case (2a). At $t = t^*$, a saturation discontinuity takes place at the interface. Let us call S^* the saturation which satisfies $F_1(S^*) = F_2(S_{w2})$. Then, when $t \geqslant t^*$ and as long as $S_1(z_0,t) < S^*$, the solution in region 2 is a shock from $S = S^+(z_0,t)$ to $S = 0$ since the concave hull over $[0,S^+(z_0,t)]$ is a straight line (Fig. 8a). As in case (1b), this shock travels upward with a velocity $v(t) = \frac{F_2(S^+(z_0,t))}{S^+(z_0,t)} > 0$. When $S_1(z_0,t)$ becomes greater than S^*, $S^+(z_0,t)$ becomes greater than S_{w2} and the solution is made of a rarefaction wave (r_2) between $S = S^+(z_0,t)$ and $S = S_{w2}$ and a shock (s_2) from $S = S_{w2}$ to $S = 0$. Fig. 8b shows the semi-analytical and numerical solutions which correspond to $t_1 < t^*$ and $t_2 > t^*$ where $S_1(z_0,t_2) > S^*$.

3.3. Layered heterogeneous porous medium

Subsurface and deep sedimentary aquifers, like Utsira aquifer at Sleipner site, are usually heterogeneous, and they may be schematically described as a permeable matrix with low-permeability layers. Therefore, we consider here an injection into a vertical column filled with a layered porous medium. Two cases are considered separately: a periodic layered medium and a heterogeneous (non-periodic) layered medium.

3.3.1. Periodic layered medium

In this section, we consider a periodic layered column where the low-permeability layers are identical, characterized by an absolute permeability k_2 and a thickness δ, and periodically distributed in the permeable matrix whose absolute permeability k_1 is greater than k_2. The distance l between two consecutive layers is greater than δ. CO_2 injection takes place at the bottom of the column at $z = 0$.

Let z_{i1} and z_{i2} be the elevations of the bottom and top of layer i, respectively ($z_{i1} < z_{i2}$), then $z_{i2} - z_{i1} = \delta$ and $z_{i+1,1} - z_{i2} = l$ (Fig. 9a). Let t_{i1} and t_{i2} be the arrival times of the CO_2 front at z_{i1} and z_{i2}, respectively. We analyze now the saturation evolution over all the intervals $[z_{i1},z_{i2}]$ and $[z_{i2},z_{i+1,1}]$.

For $t < t_{12}$, the saturation evolution over $[0,z_{11}]$ is described in case (1a): a shock (s_{12}) is created at z_{11} propagates downward and meets the rarefaction wave (r_1) (Fig. 5a). On the interval
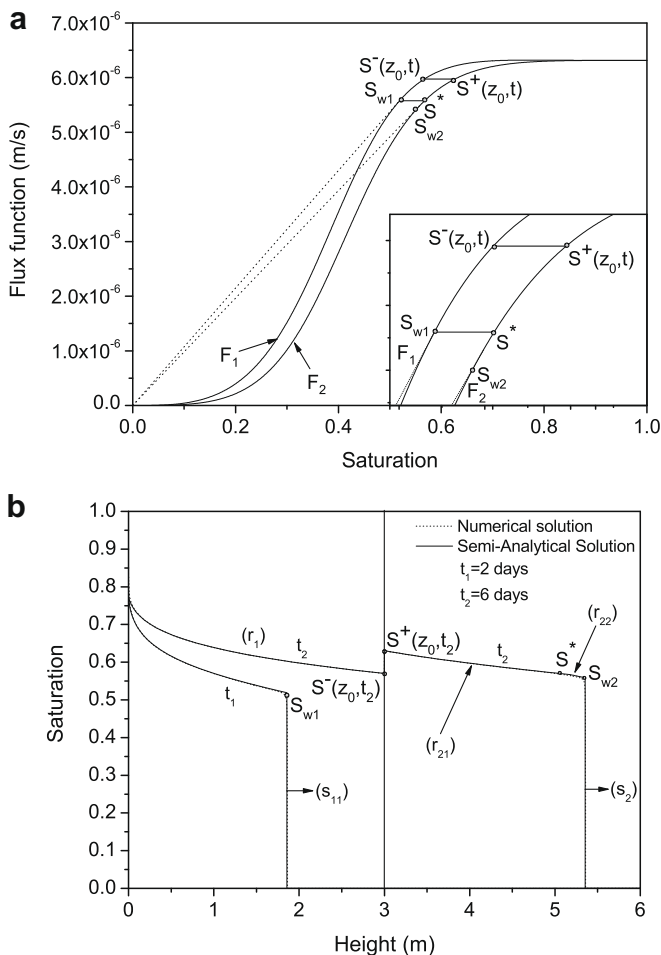

Fig. 7. CO_2 migration in a vertical column filled with a piecewise homogeneous porous medium. Case (2a) injection driven ($\theta \ll 1$) and medium one (left) is more permeable than medium two (right) ($r > 1$). (a) Flux curves, concave and convex hulls; (b) numerical and semi-analytical solutions.
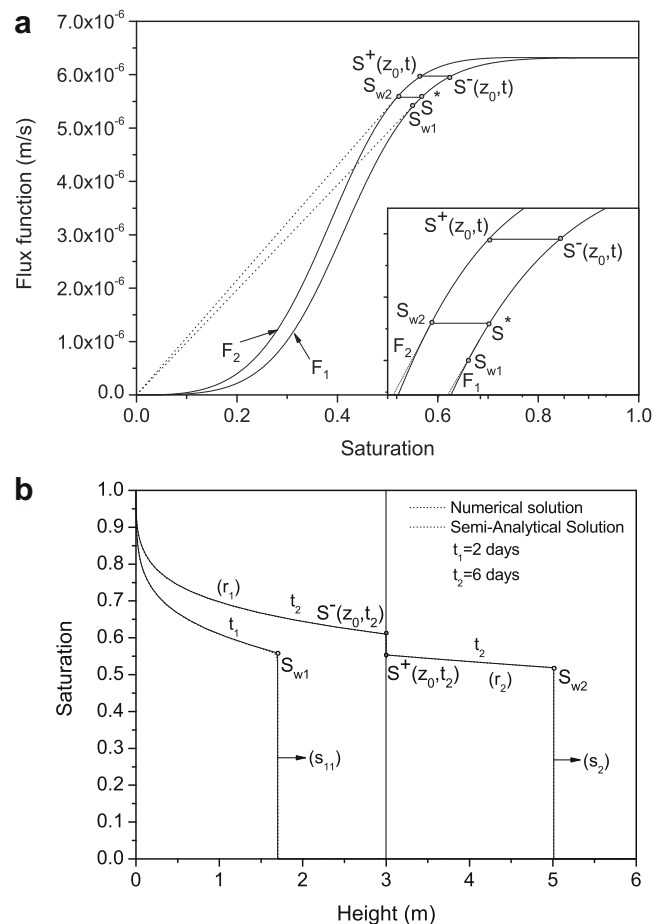

Fig. 8. CO_2 migration in a vertical column filled with a piecewise homogeneous porous medium. Case (2b) injection driven ($\theta \ll 1$) and medium two (right) is more permeable than medium one (left) ($r < 1$). (a) Flux curves, concave and convex hulls; (b) numerical and semi-analytical solutions.

$[z_{11}, z_{12}]$, a rarefaction wave (r_{21}) is created from $S = S_{max,2}$ to $S = S_{w2}$ and a shock from $S = S_{w2}$ to $S = 0$ which travels upward.

For $t > t_{12}$, the flux continuity at the interface $z = z_{12}$ implies a saturation discontinuity between two saturations $S^-(z_{12}, t)$ and $S^+(z_{12}, t)$ where $F_2(S^-(z_{12}, t)) = F_1(S^+(z_{12}, t))$. This situation is described in case (1b). Since $S^-(z_{12}, t)$ cannot exceed $S_{max,2}$, the maximal saturation value which can be reached at the interface in the permeable matrix is $S^+(z_{12}, t) = \bar{S}_{min,1}$, where $\bar{S}_{min,1}$ satisfies $F_1(\bar{S}_{min,1}) = F_2(S_{max,2})$ and $\bar{S}_{min,1} < S_{max,2}$ (Fig. 5a).

For $t < t_{21}$, and over $[z_{12}, z_{21}]$ a shock appears between $S = S^+(z_{12}, t)$ and $S = 0$ and travels upward with the velocity $v(t) = \frac{F_1(S^+(z_{12}, t))}{S^+(z_{12}, t)}$ (see case (1b)). Fig. 10a displays the saturation profile in the column for $t < t_{21}$ as obtained from simulations described at the end of the section.

When $t \geqslant t_{21}$, here again, a saturation discontinuity appears at the interface $z = z_{21}$. As $S^+(z_{21}, t) \leqslant \bar{S}_{min,1}$ the flux at this interface $F_1(S^+(z_{21}, t))$ remains (when time increases) less than the maximal flux $F_2(S_{max,2})$ of the low-permeability layers. Then, according to the previous discussion on saturation discontinuities at layer interfaces, no accumulation appears at $z = z_{21}$.

For larger t, when CO_2 has reached the top of the column, the following scenario repeated for each value of i describes the saturation distribution, as schematically represented in Fig. 9b:

- Over $[z_{i1}, z_{i2}]$: a rarefaction wave (r_{2i}) is created between $S^+(z_{i1}, t)$ and $S^-(z_{i2}, t)$.
- Over $[z_{i2}, z_{i+1,1}]$: the saturation is independent of z and equal to $S^+(z_{i2}, t)$, and it increases with time.

To obtain the rarefaction wave (r_{2i}) equations and the saturation values at the interfaces, let us write the trajectory of a given saturation.

The shock (s_{12}) and the rarefaction wave (r_1) over $[0, z_{11}]$ are discussed in case (1a). The trajectory of a saturation S belonging to (r_1) is $z_S = F'_1(S)t$ and the plume arrival time at $z = z_{11}$ is $t_{11} = \frac{z_{11}}{F'_1(S_{w1})}$.

The rarefaction wave (r_{21}) has been also previously discussed. The trajectory of a saturation $S \in [S_{w2}, S_{max,2}]$ described by (r_{21}) is given by $z_S = z_{11} + F'_2(S)(t - t_{11})$, where $S^+(z_{11}, t) = S_{max,2}$. Let us call $t_{S,i2}$ and $t_{S,i1}$ the arrival and departure times of the saturation S at $z = z_{i2}$ and $z = z_{i1}$. Then $t_{S,12}$ is given by the equality $\delta = F'_2(S)(t_{S,12} - t_{11})$.

As discussed in case (1b), the saturation in each permeable matrix layer is constant with z and evolves with time. Therefore, at larger t, we have the equality $S^+(z_{i2}, t) = S^-(z_{i+1,1}, t)$ and, as a consequence of flux continuity, $S^-(z_{i2}, t) = S^+(z_{i+1,1}, t)$ (see Fig. 9b). Consequently, the arrival time in layer i of the saturation S is equal to the departure time of this saturation in layer $i + 1$: $t_{S,i2} = t_{S,i+1,1}$. This leads to the following expression for the trajectory in layer i: $z_S = z_{i1} + F'_2(S)(t - t_{i1}) = z_{i1} - (i - 1)\delta + F'_2(S)(t - t_{11})$. Finally, the saturations at the interfaces of layer i, for a given time t, are given by the sequence of equalities $F'_2(S^-(z_{i2}, t)) = \frac{i\delta}{t - t_{11}}$ and $S^+(z_{i+1,1}, t) = S^-(z_{i2}, t)$ where $i = 1, \dots, n$, $t_{11} = \frac{z_{11}}{F'_1(S_{w1})}$ and $S^+(z_{11}, t) = S_{max,2}$.

In Fig. 10a and b, we present a comparison between numerical and semi-analytical solutions at two times, 40 and 200 days, respectively, for a periodic layered column made up of four low-permeability thin layers. The physical characteristics are given in Table 1. As we observe, a single shock propagates downward. This shock is cre-
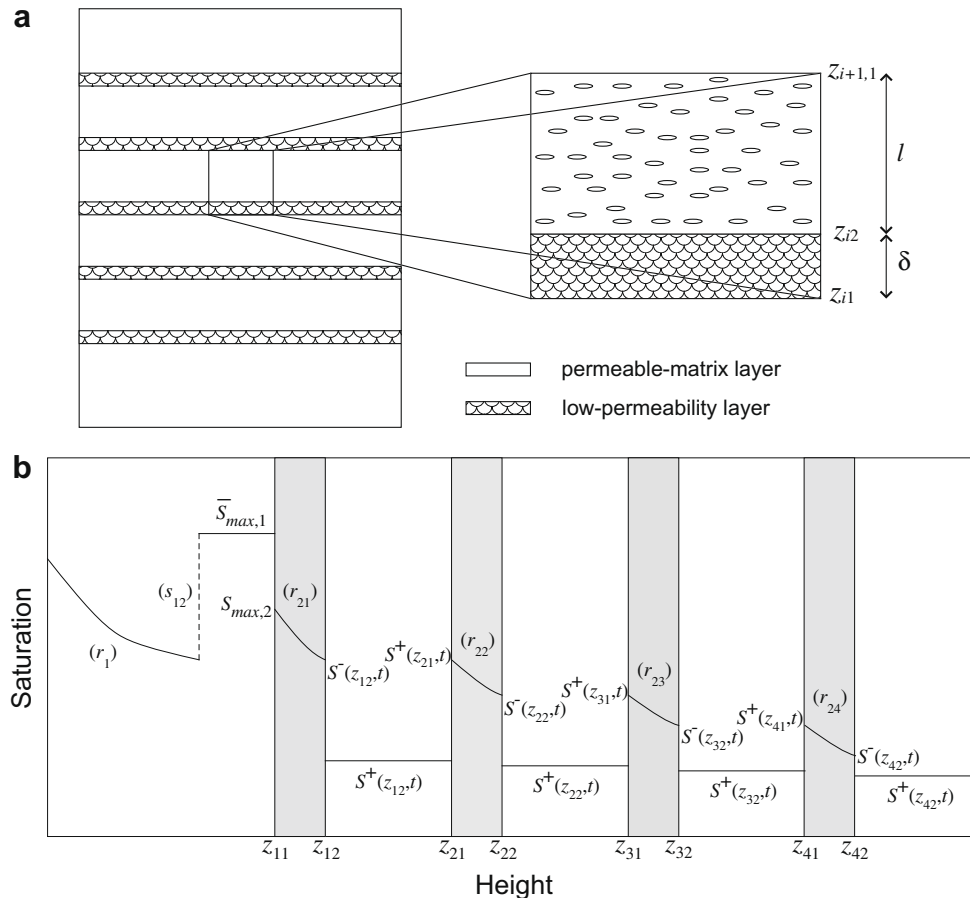

Fig. 9. Schematic representations of the periodic layered column (a) and the saturation distribution (b).
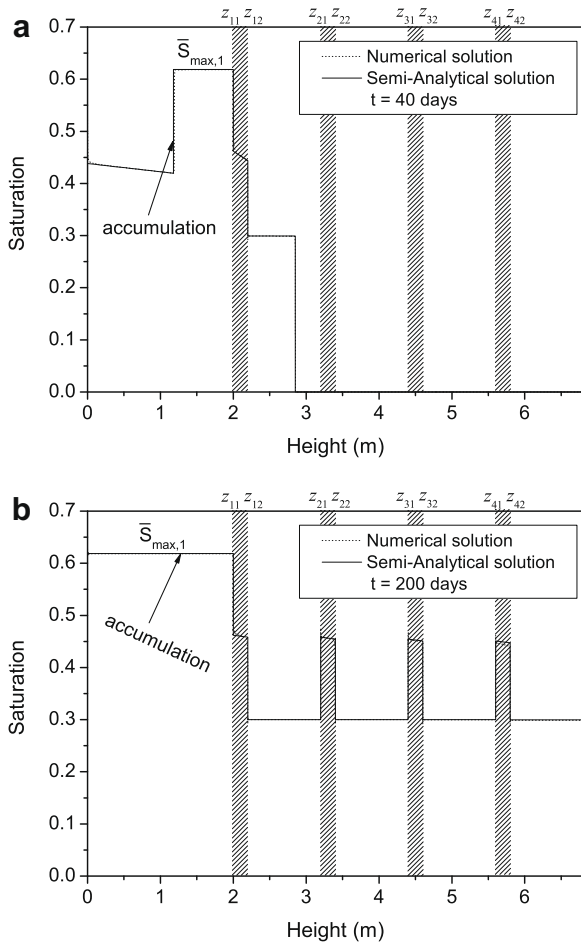
Fig. 10. CO_2 migration in a vertical column filled with a periodic layered porous medium. Numerical and semi-analytical solutions at (a) short time (40 days); (b) long time (200 days).

ated beneath the first thin layer. When time increases, this shock disappears at the bottom and the part of the domain located between $z = 0$ and $z = z_{11}$ becomes saturated with $S = \overline{S}_{max,1}$, as shown in Fig. 10b. As the saturation between two thin layers cannot exceed $\overline{S}_{min,1}$, there is no CO_2 accumulation beneath these thin layers.

From this study, we can draw the following conclusion for the case of injection into a vertical (1D) periodic column:

- The CO_2 is "filtered" by the first low-permeability layer and it is trapped with constant high-saturation $\overline{S}_{max,1}$ between the injection well and the first low-permeability layer.
- There is no CO_2 accumulation beneath the upper low-permeability layers and the saturation $S^+(z_{i2},t)$ is low (maximal value $\overline{S}_{min,1}$), constant in space and increasing in time.
- The saturation $S^+(z_{i2},t)$ decreases in each high-permeability layer (i.e. $S^+(z_{i2},t) > S^+(z_{i+1,2},t)$).
- The saturation value in each low-permeability layer varies between S_{w2} and $S_{max,2}$.

3.3.2. Non-periodic layered porous medium

As previously demonstrated, in the case of a periodic layered medium, the first low-permeability layer "filters" CO_2: saturations accumulate at a value $S = \overline{S}_{max,1}$ beneath the layer and there is no accumulation beneath the other layers. This scenario does not happen anymore in the case of a random heterogeneous porous medium. As an example, we consider the case of Fig. 11b, where the column contains two low-permeability layers of different perme-

abilities k_2 and k_3 such that $k_3 < k_2 < k_1$, where k_1 is the permeable matrix permeability. Physical parameters are given in Table 1. The flux functions for the three media are shown in Fig. 11a. We use the same definitions and notations as in previous sections.

For $t < t_{21}$, where t_{21} is the arrival time at the bottom of the second layer (permeability k_3), the saturation evolution is the same as in the case of a periodic layered medium, see Fig. 10a. CO_2 accumulates under the first layer (permeability k_2) with a saturation $\overline{S}_{max,12}$. In this layer $S \in [S_{w2},S_{max,2}]$ and in the permeable matrix, i.e. over $[z_{12},z_{21}]$, saturation is constant with z and increases with time from S^* to $\overline{S}_{min,1}$, where $F_1(S^*) = F_2(S_{w2})$ and $F_1(\overline{S}_{min,1}) = F_2(S_{max,2})$.

At $t = t_{21}$, the CO_2 front reaches the bottom of the second layer ($z = z_{21}$), with a saturation $S = S^+(z_{12},t_{21})$. Since this saturation is such that $F_1(S) \geqslant F_3(S_{max,3})$, the flux continuity cannot be respected as shown in Fig. 11a. Following case (1a): the saturation in the permeable matrix at $z = z_{21}$ becomes equal to $S^-(z_{21},t_{21}) = \overline{S}_{max,13}$ where $F_1(\overline{S}_{max,13}) = F_3(S_{max,3})$. Therefore, a shock propagates downward with a velocity $v(t) = \frac{F_1(S^+(z_{12},t)) - F_1(\overline{S}_{max,13})}{S^+(z_{12},t) - \overline{S}_{max,13}} < 0$ indicating that CO_2 accumulates also under the second layer. For $z > z_{21}$, the solution is the same as for $z > z_{11}$ (a rarefaction wave from $S_{max,3}$ to S_{w3} over $[z_{21},z_{22}]$). Fig. 11b shows a comparison between semi-analytical and numerical solutions after 100 days of injection.

These results can be generalized to the case of an injection into a heterogeneous vertical (1D) layered column. The layer which has the lowest permeability "filters" the CO_2 saturation: CO_2 accumu-
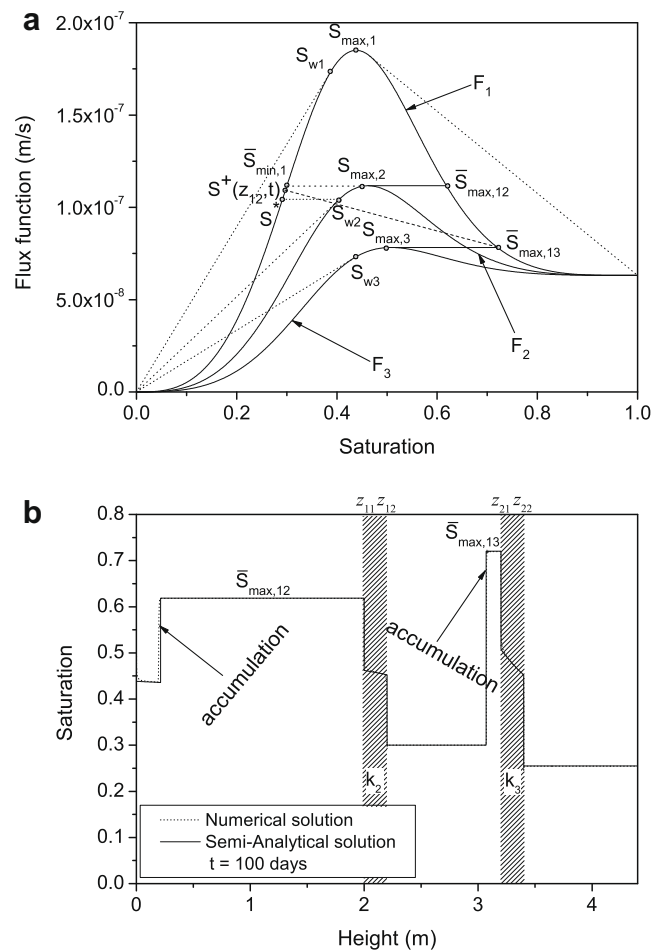

Fig. 11. CO_2 migration in a vertical column filled with a non-periodic layered porous medium. (a) Construction of the convex and concave hulls; (b) numerical and semi-analytical solutions.

lation occurs beneath this layer and may be occurs beneath lower layers but cannot occur beneath upper layers.

4. Injection and migration in a 2D stratified heterogeneous aquifer

As discussed in Section 1, one of the objectives of this work is to qualitatively explain the CO_2 plume accumulation under each mudstone layer as observed in Utsira aquifer at Sleipner Vest field. For this purpose we model Utsira as a 2D permeable aquifer containing regularly spaced identical low-permeability layers. These assumptions are common in the litterature dealing with Sleipner modeling [29]. According to the discussions made in previous sections, an accumulation under a low-permeability layer is characterized by a saturation discontinuity at the interface with $S^-(z_0, t)$ at the upstream side (in the high-permeability layer) and $S^+(z_0, t)$ at the downstream side (in the low-permeability layer) such that $S^-(z_0, t) > S^+(z_0, t)$, where z_0 is the interface coordinate. This type of saturation discontinuity comes from the fact that the upstream-flux value is greater than the maximal downstream-flux value. Then, flux continuity at the interface can only be satisfied if the upstream-flux value is reduced to a value equal to the maximal downstream-flux value. In a vertical column two cases have been distinguished: (i) if the low-permeability layers are identical, accu-

mulation occurs only beneath the first one, numbering starting at the bottom; (ii) if the low-permeability layers have different permeabilities, accumulation occurs beneath some particular layers, the most elevated layer of this sequence have the lowest permeability. The key parameter which explains the difference between this 1D accumulation mechanism and the observed 2D one, i.e. accumulation beneath each low-permeability layer, is the total velocity. Indeed, it is constant in 1D but decreases with elevation in 2D.

To prove this assertion, we consider a 2D vertical cut of Utsira and simulate the CO_2 injection in order to obtain the velocity field, then we analyze theoretically the evolution of the flux function with elevation in the vertical cut. Utsira is modeled as a 2D domain, 20 km long and 196 m thick, made of 16 m thick high-permeability sandstone layers separated by nine thin low-permeability mudstone layers (4 m thick), see Fig. 12a. The injection point is located on the left corner at the bottom of the domain. Fluid and aquifer properties are taken from the GeoSeq benchmark [27] (see Table 2). Simulation of CO_2 injection is performed with the code Cast3M.

Fig. 12b shows a zoom on the CO_2 saturation distribution at the bottom of the 2D domain, where only the first mudstone layers are represented. Fig. 13 gives the saturation profile along the vertical axis passing through the injection point, after 3 months of injection. As expected, accumulation of CO_2 is observed under each
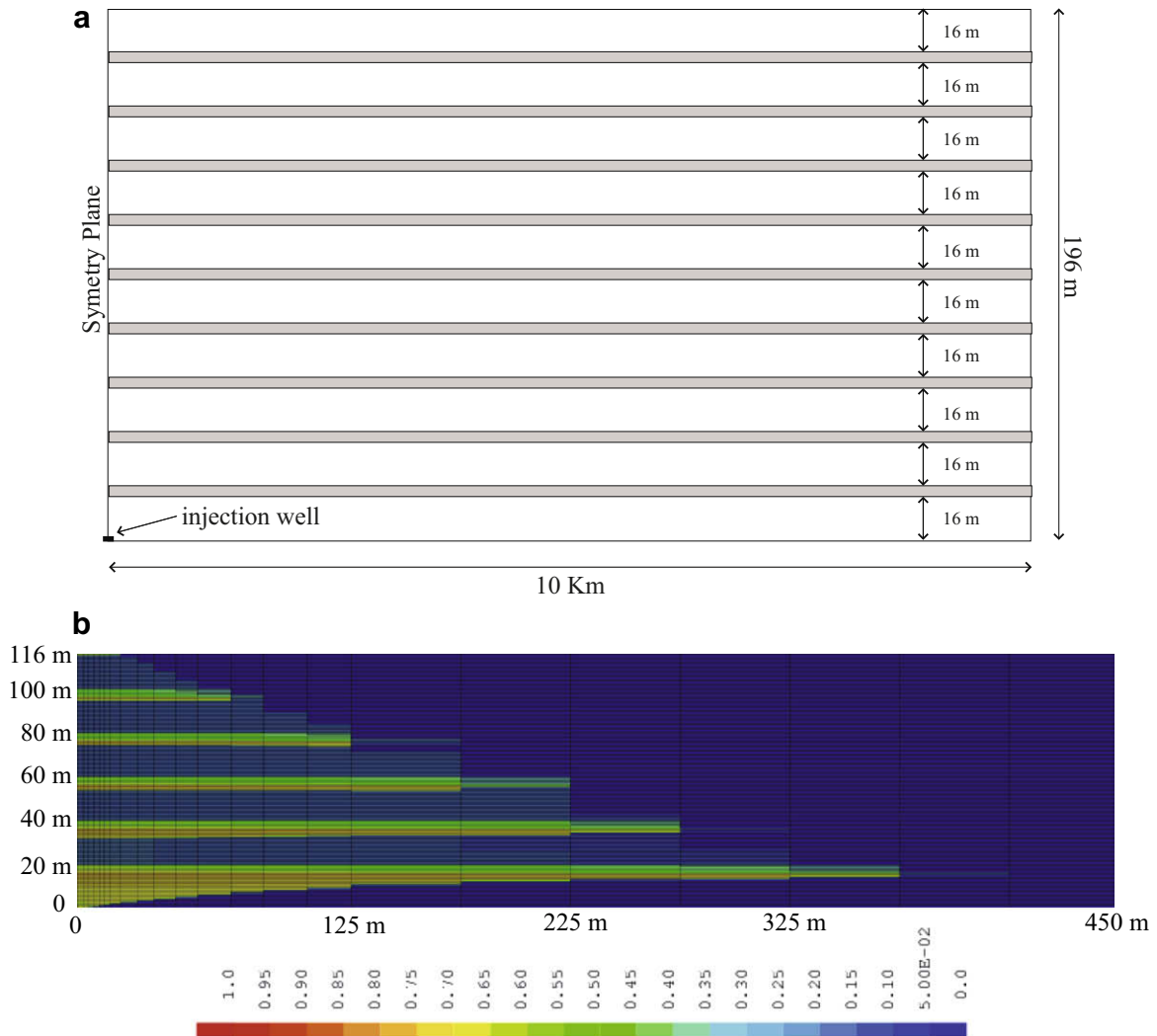

Fig. 12. (a) Schematic representation of a vertical cut of Utsira aquifer at Sleipner; (b) CO_2 saturation distribution after 3 months of injection.

Table 2
Fluid properties and parameters of aquifer simulation.

Porous media properties:	
ϕ	Sands: 0.35
	Shales: 0.35
k (m^2)	Sands: 3×10^{-12}
	Shales: 10^{-14}
Fluid properties:	
ρ_w (kg m^{-3})	997.42
ρ_g (kg m^{-3})	716.7
μ_w (kg m^{-1} s^{-1})	6.922×10^{-4}
μ_g (kg m^{-1} s^{-1})	5.916×10^{-5}
S_rw	0.2
S_rg	0.05
k_rw	Brooks–Corey
k_rg	Brooks–Corey
Initial conditions:	
S^0	0
Well boundary condition:	
S^N	0.8
q^N (kg s^{-1})	0.1585
$x = Lx$ Boundary condition:	
P^D	Hydrostatic
System geometry:	
Domain horizontal width Lx (m)	20,000
Domain vertical width Lz (m)	196
Spatial discretization:	
Cell number in x	88
Cell number in z	784
Grid resolution Δx (m)	$0.5 < \Delta x < 500$
Grid resolution Δz (m)	0.25

Fig. 14. Evolution of the velocity vertical component along the vertical axis and a zoom on this component in the region above the first mudstone layer.

mudstone layer and the thickness of accumulated CO_2 lenses diminishes with elevation. Moreover, we see that the saturation distribution is described by a rarefaction wave in mudstone layers, with a mean saturation $S = 0.6$, and by a shock in the sandstone layers, with a lower mean saturation $S = 0.2$. This saturation distribution is comparable to the one obtained for the periodic layered column (see Fig. 10b). Fig. 14 displays the vertical component of the velocity along the vertical axis. We see that this component decreases drastically at the first low-permeability layer. A zoom of this component in the region above this first layer shows that it decreases steeply just beneath each mudstone layer and is constant in the layer (see Fig. 14).

The flux function depends explicitly on saturation S and vertical coordinate z via the velocity $\mathbf{v}(x,z)$ and the absolute permeability k: $\mathbf{F}(S,x,z) = f(S)[\mathbf{v}(x,z) + k(z)(\rho_\text{w} - \rho_\text{g})g\lambda_\text{w}(S)\nabla z]$, where $k = k_\alpha$, with

$\alpha = 1$ for sandstone layers, $\alpha = 2$ for mudstone layers ($k_2 < k_1$) and where x and z denote horizontal and vertical coordinates, respectively. Let i be the index which numbers the mudstone layers from the bottom of the aquifer. For $i \geqslant 1$, we note v_i the value of the vertical velocity component in the ith mudstone layer, value assumed to be constant and taken along axis z, and we note z_{i1} and z_{i2} the elevations of the ith layer inflow and outflow surfaces, respectively. To explain the accumulation under the $i + 1$th mudstone layer, we plot schematically in Fig. 15 the vertical component of the flux function at both sides of the outflow surface $z = z_{i2}$ and inflow surface $z = z_{i+1,1}$ of the second and third mudstone layer: $F_{i,\alpha}(S) = \frac{1}{\phi_\alpha}f(S)[v_i + k_\alpha(\rho_\text{w} - \rho_\text{g})g\lambda_\text{w}(S)]$ and $F_{i+1,\alpha}(S) = \frac{1}{\phi_\alpha}f(S)[v_{i+1} + k_\alpha(\rho_\text{w} - \rho_\text{g})g\lambda_\text{w}(S)]$ where $\alpha = 1,2$ and $i = 2$. The flux function is "S-shaped" in mudstone layers and "bell-shaped" in sandstone layers. Moreover, $F_{i+1,\alpha}(S) > F_{i,\alpha}(S)$ whatever α. This remains true in the upper part of the aquifer and this is why we keep the index i in the flux indexation.

Let $\overline{S}_{min,i}$ be the saturation which satisfies $F_{i,1}(\overline{S}_{min,i}) = F_{i,2}(1 - S_\text{rw})$ (i.e. $\overline{S}_{min,i}$ is the saturation in the sandstone layer which corresponds to the maximal flux value in the $i + 1$th mudstone layer, see Fig. 15). The flux continuity at the outflow surface of the ith mudstone layer with the sandstone layer, at $z = z_{i2}$, implies that the maximal saturation value which can be reached in the
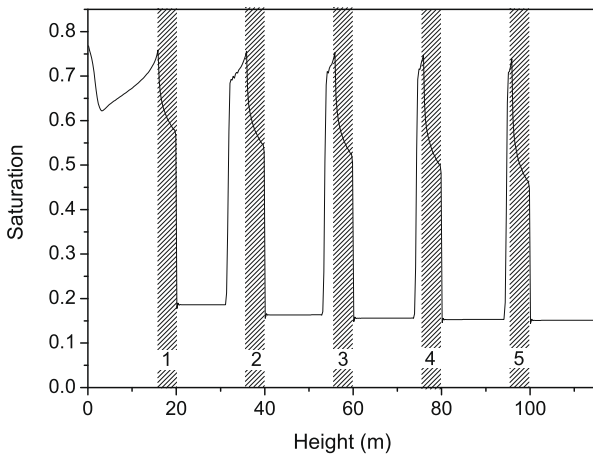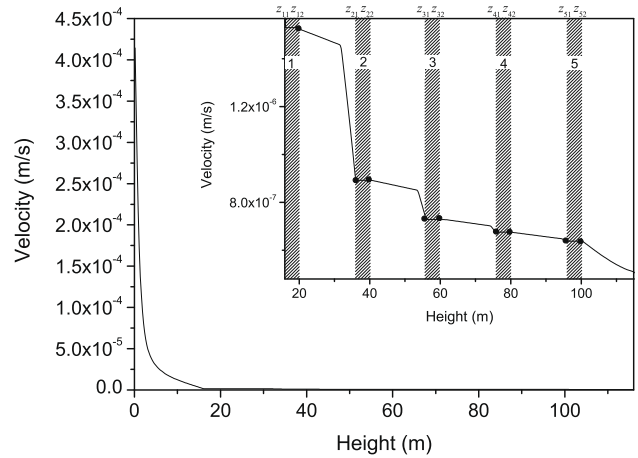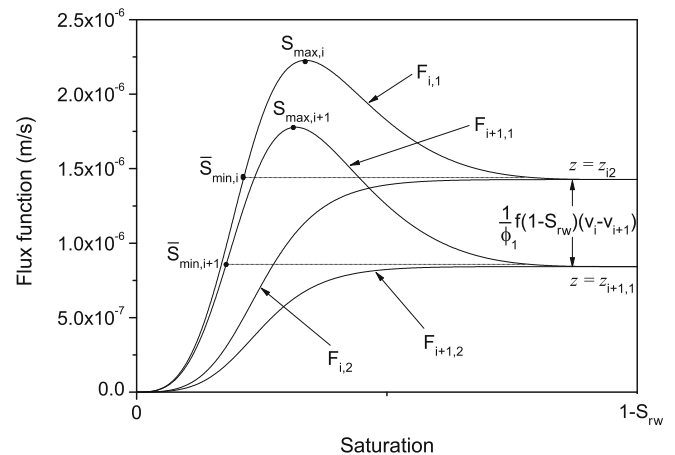

Fig. 13. Saturation profile along the vertical axis passing through the injection well.

Fig. 15. Vertical components of the flux functions at both sides of the outflow surface $z = z_{i2}$ and inflow surface $z = z_{i+1,1}$ of the second and third mudstone layers ($i = 2$). "Bell-shaped" functions correspond to sandstone sides and "S-shaped" functions correspond to mudstone sides.
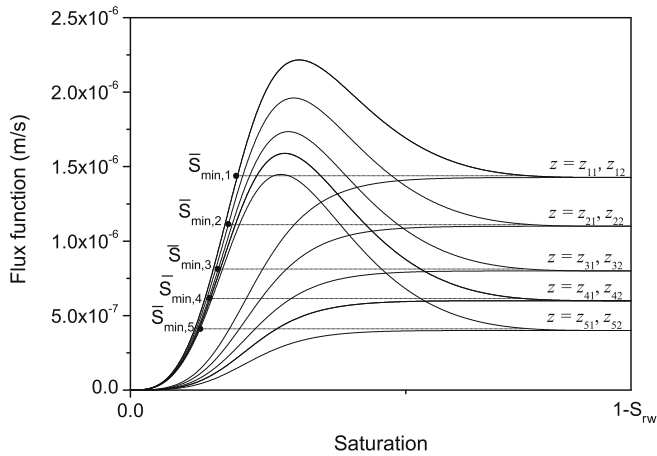
Fig. 16. Vertical components of the flux functions at both sides of the inflow surface $z = z_{i1}$ and outflow surface $z = z_{i2}$ of the first five mudstone layers. "Bell-shaped" functions correspond to sandstone sides and "S-shaped" functions correspond to mudstone sides.

sandstone layer is $\overline{S}_{min,i}$. If $\overline{S}_{min,i+1} < \overline{S}_{min,i}$, then the CO_2 plume reaches the $i + 1$th mudstone layer with a flux value greater than the maximal flux value in the $i + 1$th mudstone layer. Consequently, CO_2 accumulation takes place beneath this layer.

The inequality $\overline{S}_{min,i+1} < \overline{S}_{min,i}$ is always satisfied whatever the value of i. As a matter of fact, by definition, $\overline{S}_{min,i} < S_{max,i} < 1 - S_{rw}$ and $F_{i,1}(\overline{S}_{min,i}) - F_{i+1,1}(\overline{S}_{min,i+1}) = \frac{1}{\phi_T}f(1 - S_{rw})(v_i - v_{i+1}) > 0$ then, $\overline{S}_{min,i+1} < \overline{S}_{min,i}$. Therefore, we can write the following sequence of inequalities (see Fig. 16):

$$\overline{S}_{min,1} > \overline{S}_{min,2} > \cdots > \overline{S}_{min,n}, \tag{20}$$

where n is the number of mudstone layers ($n = 9$ in our case). Inequalities (20) show that CO_2 accumulates beneath each mudstone layer. These saturation values represent the mean level, i.e. time average, of saturation value in each sandstone layer: $\overline{S}_{min,i}$ is the mean saturation value in the sandstone layer above the ith mudstone layer. The mean saturation in the accumulation zones beneath each mudstone layer is $1 - S_{rw}$. In the 2D simulation of Utsira, we have $1 - S_{rw} = 0.8$ and $\overline{S}_{min,i}$ lies in the range 0.15–0.25, see Fig. 15. This is in agreement with Fig. 13 which shows the saturation profile along the vertical axis.

We implicitly assume in this demonstration that the saturation front which travels in the sandstone layer along the vertical axis from the ith to the $i + 1$th mudstone layers do not decrease with time from $\overline{S}_{min,i}$ to a value smaller than $\overline{S}_{min,i+1}$. As the problem is not 1D but 2D, we cannot demonstrate this assumption. Nevertheless, Fig. 15 shows that the saturations $\overline{S}_{min,i}$ and $\overline{S}_{min,i+1}$ are low and in a range where the flux function does not vary so much, showing that migration in sandstone along the vertical axis is quasi-unidimensional. Moreover, as $\overline{S}_{min,i}$ is always smaller than the Welge saturation value of the flux function $F_{i,1}$, the saturation in the sandstone layer is probably described by a shock, and therefore cannot decrease as in 1D (see case (1b) of Section 3.2).

5. Conclusion

The migration of CO_2 injected into a heterogeneous layered porous media saturated with water has been studied with a Buckley–Leverett equation with gravity. As CO_2 is less dense than water, it rises under the combined action of the injection rate and buoyancy. In a first step, we investigated the CO_2 migration in a vertical homogeneous column, and then in a heterogeneous layered column. The associated Riemann problems have been solved in each

case and, depending on the heterogeneity vertical distribution, the saturation evolution in space and time displays a large variety of migration behaviours made of shocks and rarefaction waves with saturation discontinuities at layer interfaces. We showed that when a wave (rarefaction or shock) reaches the interface with a flux value greater than the maximal flux value of the low-permeability layer, all the CO_2 carried by this wave cannot be transmitted to the low-permeability layer. Continuity of flux at the interface can only be satisfied if the flux at the interface is reduced to a value equal to the maximal flux value of the low-permeability layer. This reduction results in a reflected shock and consequently CO_2 accumulates with high-saturation value beneath the low-permeability layer. An important result is: in a one-dimensional vertical layered porous medium, the least permeable layer "filters" the CO_2 saturation, i.e. CO_2 accumulates beneath this layer and not the upper layers. For each case, semi-analytical solutions have been proposed and showed a good agreement with simulation results.

The study has been extended to the two-dimensional case, with a 2D vertical cut of a periodic layered aquifer representing schematically a vertical cut of Utsira aquifer at Sleipner site in Norway. We proposed an explanation to the observed CO_2 stratification beneath each low-permeability mudstone layer, based on the concomitant decrease of the velocity and flux function with elevation.

A next step of this work will be to take into account capillary effects. These effects should facilitate vertical migration through the low-permeability layers and compete with the stratification process. After injection one expects that these capillary effects dominate in the vertical migration.

References

[1] Adimurthi, Jaffré J, Veerappa Gowda GD. Godunov-type methods for conservation laws with a flux function discontinuous in space. SIAM J Numer Anal 2004;42(1):179–208.
[2] Allen III MB, Behie GA, Trangenstein JA. Multiphase flow in porous media. Berlin: Springer-Verlag; 1988.
[3] Bear J, Bachmat Y. Introduction to modeling of transport phenomena in porous media. Kluwer Academic Publishers; 1991.
[4] Bachu S. Geological sequestration of anthropogenic carbon dioxide: applicability and current issues. In: Gerhard LC, Harrison WE, Hanson BM, editors. Geological perspectives of global climate change. Tulsa, OK: American Association of Petroleum Geologists; 2002. p. 285–303.
[5] Bickle M, Chadwick A, Huppert HE, Hallworth M, Lyle S. Modelling carbon dioxide accumulation at Sleipner: implications for underground carbon storage. Earth Planet Sci Lett 2007;255(1–2):164–76.
[6] Bielinski A. Numerical simulation of CO_2 sequestration in geological formations. PhD thesis, University of Stuttgart, Germany; 2006.
[7] Brooks RH, Corey AT. Hydraulic properties of porous media. Hydrol paper 3, State University, Colorado; 1964.
[8] Buckley SE, Leverett MC. Mechanism of fluid displacement in sands. Trans Am Inst Miner Metall Eng 1942;146:107–16.
[9] Chavent G, Jaffré J. Mathematical models and finite elements for reservoir simulation. Amsterdam: North-Holland; 1986.
[10] Cunha MCC, Santos MM, Bonet JE. Buckley–Leverett mathematical and numerical models describing vertical equilibrium process in porous media. Int J Eng Sci 2004;42(11–12):1289–303.
[11] Helmig R. Multiphase flow and transport processes in the subsurface. Berlin: Springer-Verlag; 1997.
[12] Hesse MA, Tchelepi HA, Cantwell BJ, Orr Jr FM. Gravity currents in horizontal porous layers: transition from early to late self-similarity. J Fluid Mech 2007;577:363–83.
[13] Hesse MA, Orr Jr FM, Tchelepi HA. Gravity currents with residual trapping. J Fluid Mech 2008;611:35–60.
[14] Holloway S. Storage of fossil-fuel derived carbon dioxide beneath the surface of the earth. Annu Rev Energy Environ 2001;26:145–66.
[15] Jessen K, Kovscek AR, Orr Jr FM. Increasing CO_2 storage in oil recovery. Energy Convers Manage 2005;46(2):293–311.
[16] Kaasschieter EF. Solving the Buckley–Leverett equation with gravity in a heterogeneous porous medium. Comput Geosci 1999;3:23–48.

[17] Klara SM, Srivastava RD, McIlvried HG. Integrated collaborative technology development program for CO_2 sequestration in geologic formations. United States Department of Energy R&D. Energy Convers Manage 2003;44:2699–712.

[18] Kovscek AR, Wang Y. Geologic storage of carbon dioxide and enhanced oil recovery. I: Uncertainty quantification employing a streamline based proxy for reservoir flow simulation. Energy Convers Manage 2005;46(11–12):1920–40.

[19] Kovscek AR, Cakici MD. Geologic storage of carbon dioxide and enhanced oil recovery. II: Cooptimization of storage and recovery. Energy Convers Manage 2005;46(11–12):1941–56.

[20] Langtangen HP, Tveito A, Winther R. Instability of Buckley–Leverett flow in a heterogeneous medium. Transport Porous Med 1992;9:165–85.

[21] Lindeberg E, Zweigel P, Bergmo P, Ghaderi A, Lothe A. Prediction of CO_2 dispersal pattern improved by geologic and reservoir simulation and verified by time lapse seismic. In: Williams DJ et al., editors. Greenhouse gas control technologies. Collingwood, Australia: CSIRO Publishing; 2001. p. 372–7.

[22] Lyle S, Huppert HE, Hallworth M, Bickle M, Chadwick A. Axisymmetric gravity currents in a porous medium. J Fluid Mech 2005;543:293–302.

[23] Morel-Seytoux HJ. Two-phase flows in porous media. Adv Hydrosci 1973;9:119–202.

[24] Nordbotten JM, Celia MA, Bachu S. Injection and storage of CO_2 in deep saline aquifers: analytical solution for CO_2 plume evolution during injection. Transport Porous Med 2005;58:339–60.

[25] Oldenburg C, Pruess K, Benson S. Process modeling of CO_2 injection into natural gas reservoirs of carbon sequestration and enhanced gas recovery. Energy Fuel 2001;15(2):293–8.

[26] Proskurowski W. A note on solving the Buckley–Leverett equation in the presence of gravity. J Comput Phys 1981;41:136–41.

[27] Pruess K, Bielinski A, Ennis-King J, Fabriol R, Le Gallo Y, Garcia J, et al. Code intercomparison builds confidence in numerical models for geologic disposal of CO_2. In: Gale J, Kaya Y, editors. GHGT-6 conference proceeding. Greenhouse Gas Control Technologies; 2003. p. 464–70.

[28] Pruess K, Garcia J. Multiphase flow dynamics during CO_2 disposal into saline aquifers. Environ Geol 2002;42:282–95.

[29] Pruess K, Garcia J, Kovscek T, Oldenburg C, Rutqvist J, Steefel C, et al. Code intercomparison builds confidence in numerical simulation models for geologic disposal of CO_2. Energy 2004;29:1431–44.

[30] Riaz A, Tchelepi HA. Numerical simulation of two-phase flow in porous media. Phys Fluid 2006;18:014–104.

[31] Torp TA, Gale J. Demonstrating storage of CO_2 in geological reservoir: the Sleipner and SACS project. In: Proceedings of the GHGT7 conference, Kyoto, Japan; 2002.

[32] van Genuchten MTh. A closed-form equation for predicting the hydraulic conductivity of unsaturated soils. Soil Sci Soc Am J 1980;44:892–8.

[33] Wangen M. Vertical migration of hydrocarbons modelled with fractional flow theory. Geophys J Int 1993;115:109–31.